# Spontaneous Curvatures of Copolymer Interfaces in Poor Solvents: Monolayer Morphology

**Anne L. Larsen and Eugene M. Terentjev***

*Cavendish Laboratory, University of Cambridge, J. J. Thomson Avenue, Cambridge, CB3 0HE, United Kingdom*

*Received June 23, 2006; Revised Manuscript Received October 4, 2006*

ABSTRACT: We compute phase diagrams for dilute AB diblock copolymers in poor solvent in the strong segregation limit (SSL), as function of the copolymer volume fractions, from physics derived directly from the properties of the single diblock copolymer and the interfacial surface tension between the solvent and the copolymer. We allow both volumetric as well as stiffness asymmetry between the two diblock components. We also allow for the possibility of reversion of the morphologies, which represent a system that is continuous in polymer rather than solvent. Thereby, we can map transitions between various phases with, e.g., bicontinuous and continuous structures in either solvent or copolymer. We show that the energetically favorable morphologies in the SSL are different from the morphologies in the more studied weak segregation limit (WSL). Transitions from spherical to cylindrical and from cylindrical to bicontinuous phases are observed with increased asymmetry. A remarkable result is that spherical micelles are not favored for very asymmetric polymers except when the solvent−copolymer interaction is very low.

## 1. Introduction

It is now becoming more and more common to link polypeptides and other chains in blocks, e.g., combinations of hydrophobic polyacrylate, polystyrene, or polyisoprene, with a hydrophobic polypeptide such as polyleucine. Usually, this is done to obtain better properties for membranes applied in, e.g., encapsulation techniques and active drug delivery. Such systems can be regarded as surfactants, but with both molecular parts demixing from solvent. This results in thick membranes, which give rise to thermodynamical stability exceeding that of traditional short-chain surfactants.

Block copolymers, comprising chemically distinct chains permanently linked together, are interesting because of the diverse array of ordered phases to which both polymer theory and experiment have been directed.[1,2] The preferred morphologies arise from a competition between curvature energy, which derives from the bending elasticity of the layers, geometrical constraints such as fixed surface area and fixed enclosed volume, and a signature of the bilayer aspect. Lipids are a very important class of natural existing copolymers because in biological systems lipid bilayers form closed surfaces or vesicles in aqueous solutions to prevent any contact between the hydrocarbon chains of the lipid molecules and the water. In the same way, a diblock copolymer with chemically distinct different components will form different morphologies, shielding the most insoluble component from the solvent.

Lipid bilayers are among the most important "construction materials" for the cell.[3] A bilayer membrane constitutes a flexible barrier that separates the interior and exterior of a cell, encapsulates the nucleus, and can perform a number of roles such as acting as a functional host for protein production. Membranes appear in flat, spherical, tubular, or tortuous and possibly bicontinuous forms in the cell, depending on function and composition.[4] Lipid solution composition determines the large-scale properties necessary for the function of the particular membrane. Such properties include flexibility, stiffness with respect to bending and stretching, viscosity, overall shape, and the degree of internal order. The curvature in biological membranes is therefore a result of many physical effects in contrast to, e.g., diblock copolymer melts where the curvature is governed by the interplay between interfacial and stretching free energies, which relate directly to the copolymer asymmetry.

Curvature can furthermore be introduced by enhancing the molecular asymmetry by utilizing tri- or tetrablock copolymers. Phospholipids are naturally occurring triblocks in living cell membranes. Various block copolymer architectures (e.g., AB diblocks, ABA and ABC triblocks, and ABCA tetrablocks) have been shown to produce the same basic phases found with low-molecular-weight amphiphiles and polymer vesicles, also referred to as "polymersomes" (ref 5 and references therein). Experimental data indicate that there is in general a phases coexistence, e.g., spherical and tubular micelles will coexist in what seems to be a thermodynamically stable system. More complex structures such as "bones" or structures made up by Y-shaped junctions and linear cylinder fractions are also found in equilibrium with bilayer vesicles or more complex, continuous morphologies.[6]

The variety and complexity of membranes have resulted in overlapping studies of membranes over the past few decades, with the natural segmentation into more specific biological and general physics studies.[7] In particular, Zhulina et al.[8] presented a model for diblock copolymers, which allows swelling of the outer component by a solvent as well as partly swelling of the core component. Thereby, they are not limited to the case of poor solvent in the strong segregation limit. However, they calculate the free energy of (bilayer) vesicles as the free energy of the lamellar structure, i.e., they do not take into account the additional force arising from the bending of the membrane, and therefore their model cannot describe the existence of vesicles where the membrane thickness is of same magnitude as the radius of the vesicle.

In this work, we investigate the "monolayer morphologies" of strongly segregated copolymers in poor solvent. The lamellar morphology in this case is actually a bilayer sheet of polymer,

* Corresponding author. E-mail: emt1000@cam.ac.uk.

10.1021/ma061416l CCC: $33.50 
Published on Web 12/05/2006

which Zhulina et al. assume represents a vesicle with negligible curvature. The purpose of our work is to show that the ratio between the two interfacial energies in SSL can give rise to curvature and that it is not only the asymmetry of the copolymer that governs the curvature. This study combines the work of Zhulina et al. of spherical micellar morphologies and the work of Milner and Olmsted[9] of more complex structures and acts as a precursor for this technique applied to vesicles with spontaneous curvature in the subsequent study of bilayer morphology.

## 2. Theory

The model presented here is based on the model of Olmsted and Milner[9] (OM) for copolymer melts where the different phases are represented by assembly of different reference geometries. We investigate the four morphologies: lamellar, bicontinuous, cylindrical, and spherical. The geometric constraints of the OM model have to be slightly modified due to the change from the melt to the copolymer solution. The modifications to the governing volume balances and area functions are presented in Section 2.1. In Section 2.2, we introduce parameters describing the asymmetry of the copolymer as well as the ratio between surface free energies. We then proceed to present the modification of the original model to account for the presence of solvent in Section 2.3, and in Section 2.4, we make an addition to the model to account for the energetically unfavorable occurrence of brush compression. Finally, in Section 2.5, we discuss the occurrence of other phases and their implications on the free energy calculations.

**2.1. Geometric Considerations.** Following OM, we calculate the free energy per diblock copolymer chain, and both diblock−diblock interaction and solvent−diblock interaction are assumed to be in the strong segregation limit (SSL), i.e., $\chi N \rightarrow \infty$ such that all interfaces are sharp. In the strong segregation limit, we can ignore the translational entropy of the junction points, which scales logarithmically with molecular weight and is thus subdominant.[9]

First of all, it is convenient to define a ratio of the cross-sectional area at a height $z$ relative to that of the outer surface, in an infinitesimal geometry of height $R$:

$$a(z/R) \equiv \frac{A(z)}{A(R)} \tag{1}$$

It is important to emphasize that $R$ is not the absolute radius of the micelle but is the radius of the geometry, which is changed with the amount of solvent due to a changed volume balance. However, the absolute value of the vesicle radius will not depend on the amount of solvent (given it is a dilute system where the polymer will be present at the center of the geometry only).

The function $a(\beta)$ is equal to unity for the lamellae, $\beta$ for cylinders, $\beta(2-\beta)$ for the bicontinuous structure, and $\beta^2$ for spheres. The function can also be calculated for more complex structures.[9] In Figure 1, an illustration of the four reference geometries and the area functions is shown. In the following, the morphologies are denoted by: (S) Spherical micelles defined by three orthogonal symmetry planes, (C) cylindrical micelles defined by two orthogonal symmetry planes, (B) symmetric wedge, which closely resembles the so-called ordered bicontinuous double diamond morphology with a 3-D structure (see ref 9 for details), and (L) lamellar with one symmetry plane. We limit ourselves to the continuous morphology arising from the assembly of the symmetric wedge reference geometry because it has a relatively simple area function. The "true" bicontinuous double-diamond and the gyroid structures as well as other continuous morphologies have space-dependent area functions because the local curvature changes along the interface.

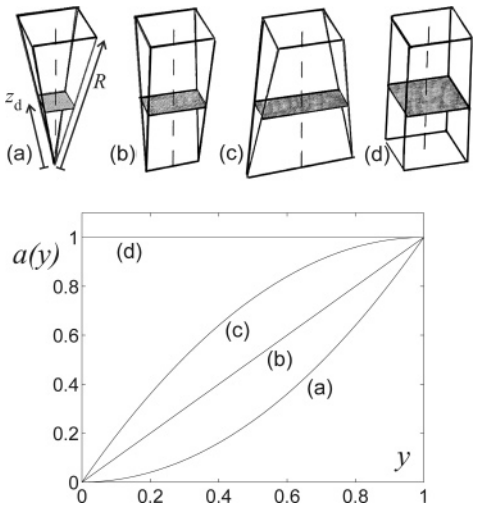


**Figure 1.** Illustration of the reference geometries and the area functions for the (a) spherical, (b) cylindrical, (c) ordered bicontinuous double diamond, and (d) lamellar morphologies. The dividing surfaces are shaded.

**Table 1. Area Functions and Volume Parameters for Different Structures**

| structure | $a(\beta)$ | $v(1)$ |
|---|---|---|
| lamellae | 1 | 1 |
| bicontinuous | $\beta(2-\beta)$ | $^2/_3$ |
| cylinders | $b$ | $^1/_2$ |
| spheres | $\beta^2$ | $^1/_3$ |

All phases are continuous in solvent, but only the B morphology is continuous in the copolymer as well. The B morphology can be thought of as a sponge of copolymer with solvent present in the continuous channels. In Section 2.5, we will discuss the reversed morphologies (denoted by $X^{rev}$, X = S, C, B), where all of the phases are continuous in copolymer rather than in solvent.

For the simple cases of a diblock copolymer melt and monolayer morphologies confined to the center of the geometry,[9] the location $z_d$ of the dividing surface is determined by setting the relative volume below the dividing surface equal to the volume fraction of the core component $\phi_B$:

$$v(z_d/R) = v(\beta) = \int_0^\beta \mathrm{d}y\, a(y) = \phi_B v(1) \tag{2}$$

where $\beta$ is the normalized distance of the dividing surface and $v(1)$ is the relative volume parameter, which is a central factor that differs from geometry to geometry:

$$v(1) = \int_0^1 \mathrm{d}y\, a(y) = \frac{V(R)}{A(R)R} \tag{3}$$

where $V(R)$ is the absolute volume of the entire geometry. The values of the relative volume parameter can be seen in Table 1. Similarly, the dividing surface between solvent and copolymer can be found from:

$$v(\beta_2) = \int_0^{\beta_2} \mathrm{d}y\, a(y) = \phi v(1) \tag{4}$$

where $\phi$ is the copolymer volume fraction ($\phi = \phi_A + \phi_B$).

With the solvent present, it is important to keep in mind that the total volume balance has changed compared to the expres-

sions in the OM model and now comprises the volume fraction of polymer:

$$\Omega = A(R)Rv(1)\phi \tag{5}$$

where $\Omega = \Omega_A + \Omega_B$ is the absolute volume of the polymer, which is a sum of the partial volumes of the two diblock species. Zhulina et al.[8] allow partial swelling of the core by the poor solvent and restrict the polymer to be in the center of the reference geometry, i.e., micellar morphologies only. The area $s$ of the dividing surface can then be obtained from a simple volume balance: $\phi_{p,c}v(1)sR_j = \Omega_B$, which gives:

$$s = a(\beta_1)A(R) = \frac{\Omega_B}{\phi_{p,c}v(1)R_j} \tag{6}$$

where $R_j$ is the radius of the core and $\phi_{p,c}$ is the volume fraction of polymer in the core. This expression is identical to ours in the case of a single-layer micelle confined in the center of the geometry and the case of no swelling of the core, i.e., $\phi_{p,c} = 1$. By introducing the area function, the surface area of a given interface $i$ in an arbitrary micellar morphology can be found by:

$$s_i = a(\beta_i)A(R) = \frac{a(\beta_i)\Omega}{v(1)R\phi} \tag{7}$$

**2.2. Introduction of Asymmetry.** To obtain a morphology diagram as function of molecular size and composition as in Jain and Bates,[6] it is convenient to define two ratios of key parameters. The compositional asymmetry ratio is defined as:

$$k_\phi = \frac{\phi_A}{\phi_B}, \qquad \phi_A + \phi_B = \phi \tag{8}$$

The surface tension ratio is defined as the ratio of the surface tension between the A species and the solvent ($\gamma_{AS}$) and the surface tension between the two species in the polymer ($\gamma_{AB}$):

$$k_\gamma = \frac{\gamma_{AS}}{\gamma_{AB}}, \qquad \gamma_{AB} + \gamma_{AS} = \gamma \tag{9}$$

The second constraint in eq 9 is not necessary, but it is found convenient in order to get same magnitude of free energies and facilitate comparison.

The end-to-end distances of the separate blocks $r_A$ and $r_B$ can be expressed in terms of the total end-to-end distance of the entire diblock for different molecular sizes and compositions (assumed Gaussian):

$$\langle r_o^2\rangle^{1/2} = \langle r_A^2\rangle^{1/2} + \langle r_B^2\rangle^{1/2} \tag{10}$$

because the diblock copolymer is assumed to possess rotational symmetry perpendicular to the contact plane of the two parts. To avoid confusion between the radius of the geometry and the polymer, we denote all radii of geometries by capital $R$ and all radii of polymer species and polymer dimensions by $r$. To correlate the end-to-end distances and thereby minimize the number of model parameters, we apply the Fredrickson's asymmetry parameter $\epsilon_F$:[10]

$$\epsilon_F = \frac{\Omega_B}{r_B^2}\frac{r_A^2}{\Omega_A} \tag{11}$$

which then expresses the end-to-end distances of the two blocks as functions of the entire equilibrium end-to-end distance of the copolymer:

$$r_A = \frac{r_o}{1 + (k_\phi\epsilon_F)^{-1/2}} \tag{12}$$

$$r_B = \frac{r_o}{1 + (k_\phi\epsilon_F)^{1/2}} \tag{13}$$

The parameter $k_\phi$ changes the volume fractions of the two polymer species relative to each other, whereas the $\epsilon_F$ changes the relative stiffness of the two (i.e., the Kuhn step length) and $r_o$ changes the overall equilibrium extension of the copolymer (i.e., its overall deviation from the simple picture of the diblock copolymer consisting of two spheres connected in one point). Thereby, we have three separate measures for the polymer asymmetry.

**2.3. The Free Energy of the Micelle.** In the strong segregation limit, the energies involved in the self-assembly of the various phases can be limited to the interfacial and the stretching free energies.[11] The free energy per molecule (in units of $k_BT$) in the strong segregation limit (SSL) can therefore be written as:

$$F = F_{int} + F_{str} \tag{14}$$

The interfacial free energy per molecule is simply the product of the surface area of one molecule at the dividing surface and the surface tension $\gamma_i$ (contains a factor of $k_BT$ implicitly), which scales with $\chi^{1/2}$ (ref 12) for every interface labeled by $i$:

$$F_{int,i} = \gamma_i A(z_i) = \gamma_i a(\beta_i)A(R) = \gamma_i\frac{\Omega a(\beta_i)}{v(1)\phi R} \tag{15}$$

The result deviates slightly from the equation in the OM model due to the changed volume balance (eq 5).

The stretching energy is calculated using the methods developed for polymer brushes and relies on an assumption of straight paths through the A−B interface.[13,14] The copolymer chains are added one by one, and the work required to add each molecule is summed. The height of the layer $h_B$, when the number of chains per area is $\sigma(h_B)$, is given by:

$$v(\beta) - v(\beta - h_B/R) = \sigma(h_B)\Omega_B a(\beta)/R \tag{16}$$

where $h_B$ is the height of the growing layer, which is growing downward in the geometry relative to the junction at $z_d$. The same can be done for the height of the layer growing upward in the geometry:

$$v(\beta + h_A/R) - v(\beta) = \sigma(h_A)\Omega_A a(\beta)/R \tag{17}$$

An important quantity is the monomer chemical potential $\mu(\phi)$, which is a decreasing function of the distance from the dividing surface and is microscopically responsible for the stretching of the chains as their monomers seek regions of lower chemical potential. Under the assumption that there are free ends at all distances from the dividing surface, the chemical potential is quadratic in the distance from the dividing surface:[15]

$$\mu(z_B) = \frac{3\pi^2}{8\Omega_B r_B^2}[h_B^2 - (z_B - z_d)^2] \tag{18}$$

For the inwardly curved parts of the structure, the assumption of the chain end density is exact. For the outwardly curved parts,

the assumption leads to an unphysical negative density of free ends but has been shown to give extremely good estimates of the stretching free energy even for layers with curvature radii comparable to their thickness.[9] The work to add a B block is independent of the location of the free end and so may be conveniently taken to be the work to add a chain with its conformation very near the surface, simply $\Omega_B u(z_d)$. Hence the total free energy of a chain is obtained by integrating up to the desired coverage:

$$F_{str} = \frac{1}{\sigma}\frac{3\pi^2}{8}\int_0^{\sigma} d\sigma' \frac{1}{r_A{}^2}h_A{}^2(\sigma') + \frac{1}{r_B{}^2}h_B{}^2(\sigma') \qquad (19)$$

From eqs 16−17, we get:

$$d\sigma = \frac{dh_B}{\Omega\phi_B'}\frac{a(\beta + h_B/R)}{a(\beta)} \qquad (20)$$

$$d\sigma = \frac{dh_A}{\Omega\phi_A'}\frac{a(\beta - h_A/R)}{a(\beta)} \qquad (21)$$

where $\phi_B' = \phi_B/\phi$ is the local volume fraction of the B species in the copolymer and similarly for A. The stretching free energy is then determined as:

$$F_{str} = \frac{\pi^2 R^2}{8\upsilon(1)\phi}\left(\frac{I_A}{\phi_A' r_A{}^2} + \frac{I_B}{\phi_B' r_B{}^2}\right) \qquad (22)$$

with:

$$I_A = 3\int_0^{\beta_2-\beta_1} dy\, a(\beta_1 + y)y^2 \qquad (23)$$

$$I_B = 3\int_0^{\beta_1} dy\, a(\beta_1 - y)y^2 \qquad (24)$$

where $\beta_1$ and $\beta_2$ are the relative positions of the A−B and the A−S interface, respectively, which are found from volume balances (eqs 2 and 4). The additional factor of $1/\phi$ in eq 22, compared to the result derived by Olmsted and Milner, comes from the changed surface coverage:

$$\sigma = \frac{\phi\upsilon(1)R}{\Omega a(\beta)} \qquad (25)$$

The free energy (eq 14) can then be written as:

$$F(R) = K_{str}R^2 + \frac{K_{int}}{R} \qquad (26)$$

where $K_{str}$ and $K_{int}$ are given by:

$$K_{str} = \frac{\pi^2}{8\upsilon(1)\phi}\left(\frac{I_A}{\phi_A' r_A{}^2} + \frac{I_B}{\phi_B' r_B{}^2}\right) \qquad (27)$$

$$K_{int} = \frac{\Omega[\gamma_{AB}a(\beta_1) + \gamma_{AS}a(\beta_2)]}{\upsilon(1)\phi} \qquad (28)$$

Here, $r_A$ and $r_B$ are constant (properties of the equilibrium copolymer), while $R$ is the radius of the full geometry, which is dependent on the total volume ratio of solvent and polymer.

Minimization of the free energy (eq 26) with respect to the internal parameter $R$ gives:

$$R_{min}{}^3 = \frac{K_{int}}{2K_{str}} \qquad (29)$$

**Table 2. Stretching Integrals for the Different Morphologies**

| | $I_A$ | $I_B$ |
|---|---|---|
| L | $(\beta_2 - \beta_1)^3$ | $\beta_1{}^3$ |
| B | $(-\beta_2 + \beta_1)^3(6\beta_2{}^2 + 3\beta_2\beta_1 + \beta_1{}^2 - 15\beta_2 - 5\beta_1)/10$ | $-\beta_1{}^4(\beta_1 - 5)/10$ |
| C | $^3/_4\beta_2{}^4 - 2\beta_2{}^3\beta_1 + {}^3/_2\beta_2{}^2\beta_1{}^2 - {}^1/_4\beta_1{}^4$ | $\beta_1{}^4/4$ |
| S | $^3/_5\beta_2{}^5 - {}^3/_2\beta_2{}^4\beta_1 + \beta_2{}^3\beta_1{}^2 - {}^1/_{10}\beta_1{}^5$ | $\beta_1{}^5/10$ |

The absolute radius of the micelle can be calculated as:

$$r = \beta_2 R_{min} \qquad (30)$$

and by inserting the optimized value of $R$ into eq 26, the value of the micellar free energy is obtained:

$$F_{mic} = (2^{1/3} + 2^{-2/3})\cdot K_{str}{}^{1/3}\cdot K_{int}{}^{2/3} \qquad (31)$$

To facilitate comparison, it is found convenient to normalize all free energies by the free energy of a completely symmetric copolymer in the melt state, i.e., $F^* = F_L(k_\phi = k_\gamma = \epsilon_F = \phi = 1)$, which is given by:

$$F^* = (2^{-1/3} + 2^{-4/3})\left(\frac{\pi\Omega\gamma_o}{r_o}\right)^{2/3} \qquad (32)$$

and is obtained from $\gamma_{AB} = \gamma_o$, $\gamma_{AS} = 0$, and $r_A = r_B = r_o/2$. The normalized free energy expression can be written as:

$$F/F^* = (K_{str}^*)^{1/3}(K_{int}^*)^{2/3} \qquad (33)$$

with the new constants expressed as function of the two parameters $k_\phi$ and $k_\gamma$:

$$K_{str}^* = \frac{1 + k_\phi}{2\upsilon(1)\phi}\left(\frac{I_A(1 + [k_\phi\epsilon_F]^{1/2})^2}{k_\phi} + I_B(1 + [k_\phi\epsilon_F]^{-1/2})^2\right) \qquad (34)$$

$$K_{int}^* = \frac{1}{\upsilon(1)\phi}\left[a(\beta_1)\frac{1}{1 + k_\gamma} + a(\beta_2)\frac{k_\gamma}{1 + k_\gamma}\right] \qquad (35)$$

with the usual expressions for the integrals $I_A$ and $I_B$ (Table 2) given in eqs 23−24. In addition, it is convenient to normalize the minimized radius of the geometry by a modified contour length. We define the characteristic length scale, which is essentially a modified contour length, as:

$$R^* = \Omega\gamma_o \qquad (36)$$

which can be seen to scale with the number of monomers in the copolymer $N$ when the monomer sizes of both species are equal because $\Omega = \Omega_A + \Omega_B = N_A a_A{}^3 + N_B a_B{}^3$, where $a_A{}^3$ and $N_A$ are the volume and number of monomers, respectively, of component A. Note that the free energy scale $F^*$ depends on the ratio $(\Omega\gamma_o)/r_o$, which is a measure of how stretched the subchains are when grafted on the interface. When examining the scaled $F/F^*$, the absolute values of $r_o$, $\Omega$ , and $\gamma_o$ do not influence the values of the relative free energy and the relative radius of the micellar structure. Thereby, we only have to account for their relative magnitudes.

**2.4. Compressional Forces.** In the above equations, we did not take into account that the optimized geometry may lead to compression of either of the diblock species brushes. To ensure that there is no such compression in any layer, or equivalently, chain extension, each layer thickness as found from the solution of eq 33 is compared to the equilibrium end-to-end distance. The resulting constraints can be written:

$$(\beta_2 - \beta_1)R_{\min} \geq r_A \tag{37}$$

$$\beta_1 R_{\min} \geq r_B \tag{38}$$

where $R_{\min}$ is the value of $R$ that minimizes $F$ (in eq 29).

When the equilibrium end-to-end distance of either of the diblock species in each corresponding brush has been reached, it is necessary to either include uniaxial compressional forces or by other means take into account that the free energy calculated is not representative for the true system. There are two scenarios occurring at each end of the polymer asymmetry limits. We therefore define two thresholds, namely $k_\phi^{\text{low}}(k_\gamma)$ and $k_\phi^{\text{up}}(k_\gamma)$, which give the lower and upper bounds for the solution of the free energy expression in eq 33 where there is no compression occurring. We then know that, for $k_\phi < k_\phi^{\text{low}}$, we have compression of the outer brush (A), and for $k_\phi > k_\phi^{\text{up}}$, we either have compression of the core component (B) or the outer species (A). The compression of A for $k_\phi > k_\phi^{\text{up}}$ is not immediately obvious, but can be explained by the fact that compression of the core component B in B, C, and S morphologies is very unlikely due to the shapes of the reference geometries. The minimization of the free energy for $\phi_B'$ can however give very wide reference geometries and thereby lead to compression of the outer species. We shall return to this delicate point later when discussing the aggregation morphologies in Section 3.1.

Because of the larger energies required to compress rather than extend polymers, we do not take into account compressional forces, but rather force the solution to the threshold of compression. The free energy for systems with $k_\phi^{\text{low}} < k_\phi$ is then calculated by forcing the radius of the outer component to the threshold in eq 37 and then calculating the free energy of the resulting system, where the core component has been stretched additionally to fit into the new thinner reference geometry.

The free energy expression can then for $k_\phi < k_\phi^{\text{low}}$ and $k_\phi > k_\phi^{\text{up}}$ in general be written as:

$$F = F_{\text{str,B}}(R^*) + F_{\text{str,A}}(R^*) + F_{\text{int}}(R^*) \tag{39}$$

where $R^*$ is the radius of the geometry calculated at the brush compression threshold. This procedure ensures continuity of the free energy expression because $\lim_{r\to r_{A+}} F = \lim_{r\to r_{A-}} F$ and $\lim_{r\to r_{B+}} F = \lim_{r\to r_{B-}} F$, where $r = \beta R$.

**2.5. Other Morphologies.** In the model, $\phi$ is not used as a tuneable parameter because the value of $\phi$ does not change the free energy per polymer molecule. It only changes the value of the relative positions $\beta_i$ as well as the radius of the geometry under the constraint resulting directly from the model that $\beta_i R$ is constant, i.e., the radius of the micelle does not change upon dilution in poor solvent.

Because we are presently discussing monolayer morphologies, it is very obvious to consider the monolayer vesicles, which are defined by three dividing surfaces ($\beta_1$, $\beta_2$, $\beta_3$) where the two outer surfaces, $\beta_1 > 0$ and $\beta_3 < 1$, are constrained. It can, however, easily be shown from scaling that monolayer vesicles are not thermodynamically favorable in the strong segregation limit, and the derivation of such scaling for the cylindrical geometry is shown in the Appendix.

In the model, we have applied the simplification that the system is so dilute that the polymer will always segregate in the center of the geometry, i.e., that the outer component of the polymer always splays outward. However, for very asymmetric polymers with A being the minority component, this curvature is not favorable. Therefore, we need to include the free energy expressions for these situations where the polymer suddenly forms the continuous phase as well. The only things changing are the integrals in the stretching free energy expression as well as the calculations of the relative positions of the surfaces $\beta_i$. The relative positions would then have to be found from:

$$\upsilon(1) - \upsilon(\beta_2) = \int_{\beta_2}^{1} \mathrm{d}y\, a(y) = \phi_B \upsilon(1) \tag{40}$$

$$\upsilon(1) - \upsilon(\beta_1) = \int_{\beta_1}^{1} \mathrm{d}y\, a(y) = \phi \upsilon(1) \tag{41}$$

The free energy can then be calculated from eq 33 with $K_{\text{str}}^*$ given by eq 34 with the integrals $I_A$ and $I_B$ given by:

$$I_A^{\text{rev}} = \int_0^{\beta_2-\beta_1} \mathrm{d}y\, a(\beta_2 - y)y^2 \tag{42}$$

$$I_B^{\text{rev}} = 3\int_0^{1-\beta_2} \mathrm{d}y\, a(\beta_2 + y)y^2 \tag{43}$$

and the normalized interfacial constant $K_{\text{int}}^*$ given by:

$$K_{\text{int}}^{\text{rev}*} = \frac{1}{\upsilon(1)\phi}\left[a(\beta_2)\frac{1}{1+k_\gamma} + a(\beta_1)\frac{k_\gamma}{1+k_\gamma}\right] \tag{44}$$

The resulting morphology is continuous in the copolymer but not in the solvent, i.e., it resembles "Swiss cheese" for spherical morphology with the area function $a(y) = y^2$. Again, we have to check for compressed solutions. Equations 37−38 are changed to:

$$(\beta_2 - \beta_1)R_{\min} \geq r_A \tag{45}$$

$$(1 - \beta_2)R_{\min} \geq r_B \tag{46}$$

The reversed geometries do depend on the dilution, in contrast to the geometries in Section 2.3, due to the solvent being present in the inner part of the reference geometry, where the reference geometry is just elongated outward for increased amount of solvent but with absolute area of the interface kept constant. For very dilute solutions, the curvature of the reversed morphology will become negligible because the inner part of the geometry contains all the solvent and the geometry will therefore become very long and thin and the free energy will not depend strongly on the dilution.

Other relevant phases are bilayers with curvatures (vesicles, etc.) and morphologies resulting from macroscopic phase separation, both of which will be discussed in detail in the following paper.[17]

## 3. Results and Discussion

Because of the shape differences in the volumes occupied by A and B in the different morphologies, the optimized absolute thicknesses of the layers (i.e., $\beta_1 R$ and $[\beta_2 - \beta_1]R$) do not follow a similar pattern as the volume fraction parameter is changed. It turns out that the spherical morphology (i.e., monolayer micelles) is not favorable for very asymmetric copolymers due to the low degree of stretching of the outer species A, and therefore the interfacial energies are very high. In Figure 2, the optimized, normalized thickness of the outer layer is shown for the four different morphologies when compression is allowed. The stretching of the core component is clearly very different for the four phases except for very large compositional asymmetries ($k_\phi \gtrsim 10^4$), but the B and C morphologies are very similar in general. The spherical morphology requires more than 2 times as much stretching of the core component than the

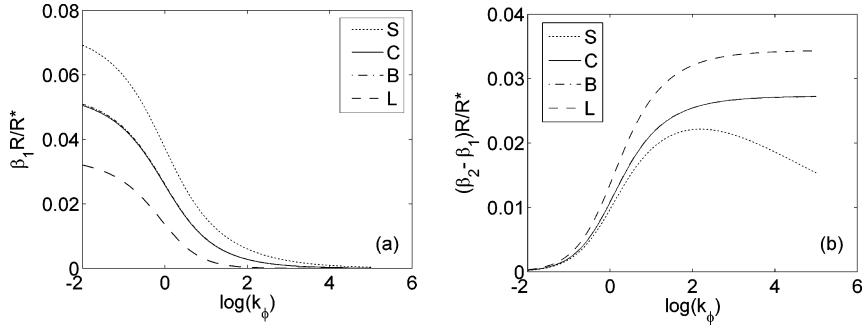


**Figure 2.** Normalized absolute thicknesses of the micellar layers for the four morphologies: (a) The core and (b) the outer layer in the geometry when the layers are allowed to be compressed; compare with Figure 3 where the compression constraints are applied for the same system. $r_o/R^* = 0.01$, $\gamma = \Omega = k_\gamma = \epsilon_F = 1$. The B and C morphologies are more or less coincident.

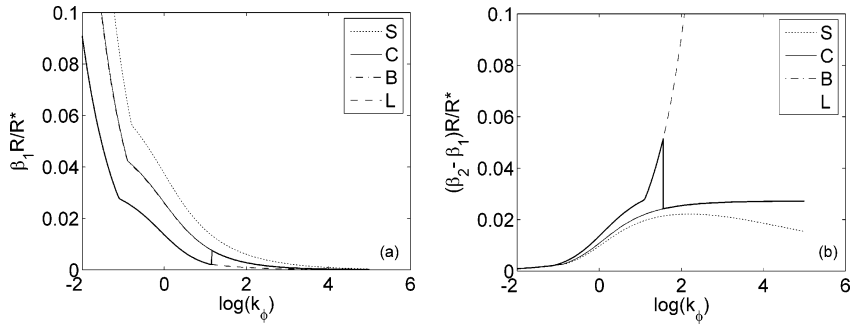


**Figure 3.** Normalized absolute thicknesses of the micellar layers when the constraints in eqs 37−38 are applied: (a) the core and (b) the outer layer in the geometry; $r_o/R^* = 0.01$, $\gamma = \Omega = k_\gamma = \epsilon_F = 1$. The B and C morphologies are more or less coincident. The thick line in both plots traces the radius of the thermodynamically stable morphology; the vertical "jumps" indicate the change in radius at the L → B transitions, which are clearly discontinuous.

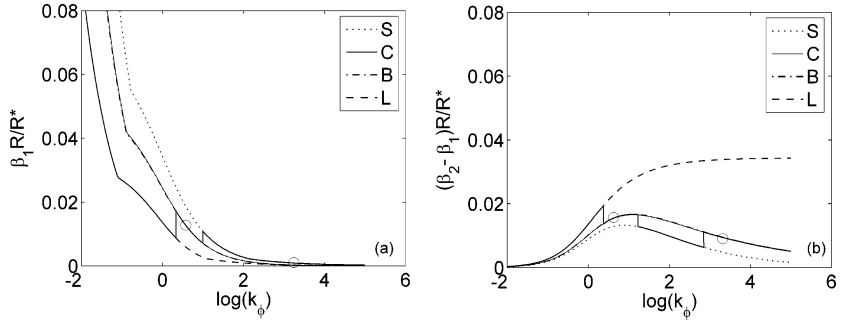


**Figure 4.** Normalized absolute thicknesses of the micellar layers for $k_\gamma = 0.001$ when the constraints in eqs 37−38 are applied: (a) the core and (b) the outer layer in the geometry; $r_o/R^* = 0.01$, $\gamma = \Omega = \epsilon_F = 1$. The B and C morphologies are more or less coincident. The thick line in both plots traces the radius of the thermodynamically stable morphology; the vertical "jumps" indicate the change in radius at the (from the left) L → B, C → S, and S → C transitions, which are clearly discontinuous. The B → C and C → B transitions are marked with a "○".

lamellar geometry. It is also evident that the stretching of the outer (A) species in the four different phases is comparable for $\log(k_\phi) < -1/2$, but for larger values of $k_\phi$, the difference becomes very significant with almost up to a factor of 2 between the lamellar and the spherical cases, but with the outer component in the spherical morphology experiences less stretching than that of the lamellar morphology. However, the lamellar morphology will experience compression of the B species for $k_\phi \gg 1$. In Figure 3, the absolute thickness of the two layers in the micelles is shown when the compression constraints (eq 39) are applied for the same system, characterized by $r_o/R^* = 0.01$. It can be seen that the inner component is compressed at small values of $k_\phi$ for all morphologies, leading to an increased thickness of the core layer when passing the compression threshold, i.e., for $k_\phi < k_{\phi,I}^{low}$, I = S, C, B, L, where $k_{\phi,S}^{low} < k_{\phi,C}^{low} < k_{\phi,B}^{low} < k_{\phi,L}^{low}$. For large values of $k_\phi$ at the given conditions, it is only the L morphology that leads to compressed solutions, which can be seen by the large increase in the thickness of the outer layer of the lamellar morphology when exceeding the compression threshold for the geometry ($k_\phi > k_{\phi,L}^{up}$). The model furthermore predicts the radius of the polymer to be discontinuous at the morphology transitions, as first shown in the weak segregation limit by Zhulina et al. The transition between the lamellar and bicontinuous phases as determined from the intersection of the two free energies has been indicated in Figures 3 and 4 for different values of $r_o/R^*$. The thickness of the inner and outer layers as function of the volumetric asymmetry for a system with several phase transitions (L → B, B → C, C → S, S → C, and C → B) is shown in these plots. In contrast to L → B, it is clear that the B ↔ C transitions that appear in the system with smaller $r_o/R^*$ (i.e., subchains closer to the mushroom regime) do not involve large changes of thickness of either layer. This is due to the close resemblance of the area function for these two phases.

Because of the normalization of $F$ with $F^*$, the values of $r_o$, $\gamma_o$, and $\Omega$ do not influence the absolute value of $F/F^*$ if compression is allowed, as seen in the OM model for the A−B diblock melt, and thereby it does not influence the morphology

transitions. However, if compression is not allowed, the values of $r_o$, $\gamma_o$, and $\Omega$ determine the threshold values $k_\phi^{low}$ and $k_\phi^{up}$, and thereby the value of $F/F^*$ depends on the parameters for $k_\phi < k_\phi^{low}$ and $k_\phi > k_\phi^{up}$, which may influence the morphology transitions.

The spherical morphology is not very favorable for dilute systems because the two interfaces in the spherical geometry will be significant larger than the two interfaces of, e.g., lamellar systems. Spherical morphologies are favorable for melts of asymmetrical copolymers due to resulting small size of the A−B interface and the "free" outer A−A surface. However, the outer surface with high tension in the spherical geometry is suddenly limiting the existence of the spherical micelles in dilute systems. The existence of spherical micelles requires a very low surface tension between the solvent and the outer speciesof the copolymer (i.e., $k_\gamma \ll 1$). From simple volume calculations, it can be shown that the area of the A−S interface is related as follows:

$$A_{2S} = \frac{3R_L}{R_S} A_L \tag{47}$$

So it is clear from Figure 2b that the spherical morphology in general is very unfavorable for systems without a large difference in interfacial energies because the spherical morphology requires 3 times as much stretching to give the same surface area as in the lamellar morphology (or $^3/_2$ as much stretching as in the cylindrical morphology). The above result is in contrast to the result of Zhulina et al. because they allow swelling of the outer component, and thereby there is not the large interfacial penalty for the spherical micelle. It is, however, important to emphasize that the model presented here is for the strong segregation limit and therefore deals with sharp interfaces only.

For values of $k_\gamma > 1$ and $\epsilon_F = 1$, it can be shown in general that the only morphology where the core component B is compressed is lamellar. The missing compression in the other phases can be explained by the geometries, where B is always confined to the more narrow part of the geometries and therefore compression will require an extremely small radius of the reference geometry (i.e., increase the interfacial energies). The model has some limitations because it requires assembly of thin geometries for the actual curvature of each reference geometry to be negligible, but the compressional constraints do in fact ensure that we do not enter the regime where the reference geometry is wider than it is long.

In general, the assumption of highly stretched chains in the monolayer morphologies is reasonable because the minimization gives stretched conditions for both chains, i.e., $r_A^2/r_o^2 > 1$ and $r_B^2/r_o^2 > 1$. For very asymmetric chains, there is a tendency to one of the chains being highly stretched and the other closer to the mushroom regime, but the free energy expression will be dominated by the stretching free energy of the highly stretched part. The assumption of the sharp interface is in this case of course not correct, but again, the stretching free energy of the highly stretched part dominates the free energy even if the interfacial area is increased. The introduction of the compressional constraint furthermore eliminates solutions where one of the parts is "compressed" below the mushroom regime.

The reversion of the reference geometry leads to a variety in morphologies with distinctly different properties than the micellar phases because the systems suddenly become continuous in polymer rather than in solvent. In Figure 5, the two spherical monolayer phases are compared at three different values of the surface tension ratio to show the competition between the energies involved in the two morphologies. The spherical micelle is preferred for geometrical reasons (when $k_\phi > 1$), but the spherical continuous morphology is preferred for interfacial energy reasons because it reduces the A−S interface. However, the competition is more likely to be between L and $S^{rev}$ when the A−S interfacial tension dominates ($k_\gamma > 1$) because both morphologies have relatively small A−S interfaces.

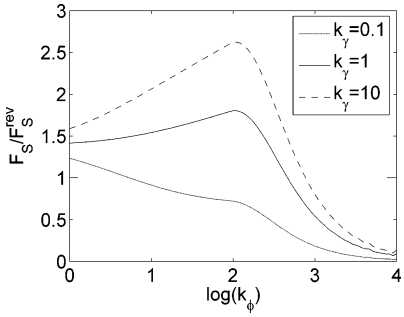


**Figure 5.** Comparison of the free energies of the two morphologies S and $S^{rev}$ described by the spherical area function. The geometrical constraints favor the S morphology, whereas the $S^{rev}$ is favored by the reduction in interfacial energy due to the reduced interfacial area. $\gamma_o = \Omega = \epsilon_F = 1$, $r_o/R^* = 0.05$, and $\phi = 0.01$.

A trend in available experimental data is the coexistence of many phases in what seems to be thermodynamically stable systems. The coexistence of, e.g., S−C and C and bilayer vesicle, is the rule rather than the exception.[16] The present model predicts the free energies of several morphologies to be more or less coinciding for certain systems, which can be seen from Figure 6, where the free energies of the four phases (systems where the A−B surface tension is dominant, i.e., $k_\gamma = 0.03$) are compared. For low values of $k_\phi$, the lamellar morphology dominates, and then the bicontinuous takes over for $k_\phi \gtrsim 2$. From the enlargement, Figure 6b, it is however very clear that the three morphologies (B, C, and S) have very similar free energies for a large range of compositional asymmetries ($2 \lesssim k_\phi \lesssim 100$). This can explain the variety of coexisting phases reported in the literature because the driving force in the kinetics will be vanishing between these morphologies. Combinations of these three phases can easily be imagined to form a huge variety of morphologies with, e.g., continuous polymer sponges with pending structures and free-floating complex structures formed from the combination of tubular and spherical micelles.

**3.1. Phase Diagrams.** In the system of AB diblock copolymer in poor solvent for both components, where the brush compression is not allowed, the morphology diagrams will depend on the overall stiffness of the copolymer ($r_o/R^*$), the stiffness asymmetry between the two copolymer parts ($\epsilon_F$), the relative volume fraction of the two components ($k_\phi$), and the relative surface energies of the A−B and the A−S interfaces ($k_\gamma$). In Figure 7, morphology diagrams for four different values of the normalized end-to-end distance of the copolymer ($r_o/R^*$) for a copolymer with no stiffness asymmetry (i.e., $\epsilon_F = 1$) can be seen. The reversed morphologies are eliminated for clarity. For very overall stiff polymers (represented by $r_o/R^* = 0.05$), the bicontinuous morphology plays a significant role for $\log k_\gamma > -1$. Only for very symmetric copolymers, the lamellar morphology dominates. When the amount of A (i.e., $k_\phi$) is increased, the A species in the lamellar morphology is stretched before the bicontinuous morphology takes over. This transition from stretched lamellar to bicontinuous is the upper convex part of the L → B transition line.

In Figure 8, it is illustrated how the value of $r_o/R^*$ influences the transition between lamellar and bicontinuous phases. For

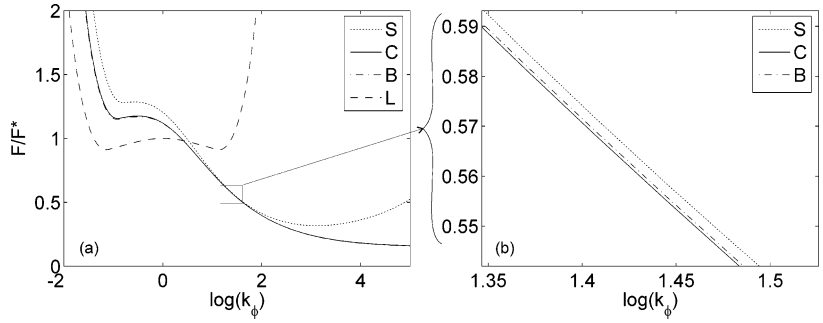


**Figure 6.** Illustration of the normalized free energies for the four micellar morphologies for a system where the surface tension of the A−S is lower than that of the A−B interface ($k_\gamma = 0.03$). Plot (b) is an enlargement of the central part of plot (a) where three of the morphologies (B, C, and S) more or less coincide. The cylindrical micelle has the lowest energy, but because of the close resemblance of the free energy with the two others morphologies, coexistence of all three phases is very likely. $r_o/R^* = 0.01$, $\gamma = \Omega = \epsilon_F = 1$.

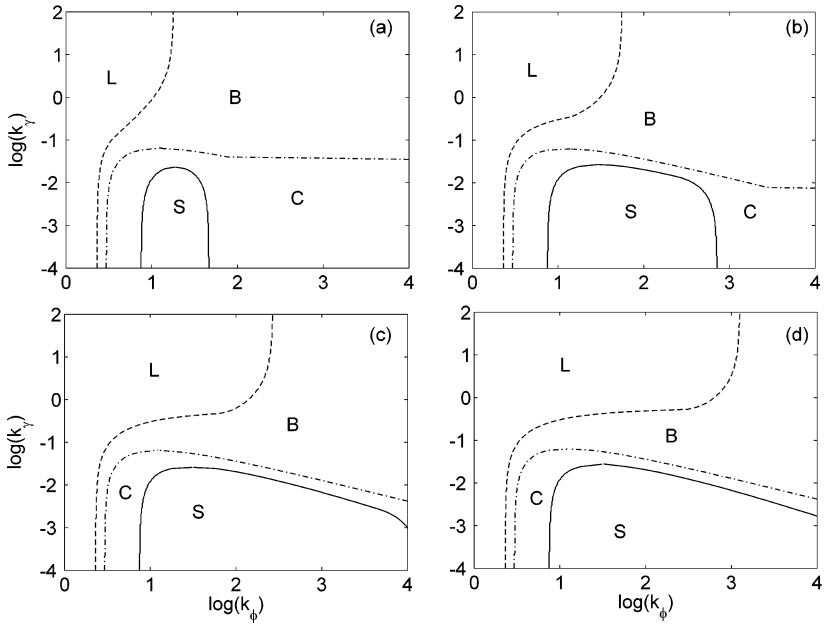


**Figure 7.** Phase diagrams for different values of the end-to-end distance of the copolymer, $r_o$, reflecting the decreasing degree of subchain stretching on the interface. (a) $r_o/R^* = 0.05$, (b) $r_o/R^* = 0.01$, (c) $r_o/R^* = 0.001$, and (d) $r_o/R^* = 0.0001$. $\epsilon_F = \gamma_o = \Omega = 1$.

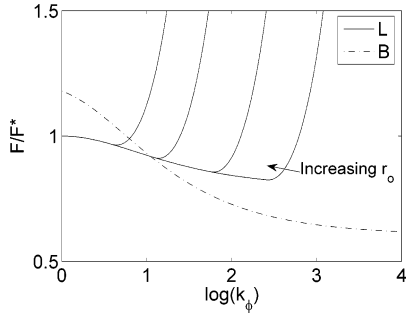


**Figure 8.** Illustration of the L−B transition for $\gamma = \Omega = 1$, $\log(k_\gamma) = -1/2$, and four different values of $r_o/R^*$: $r_o/R^* = 0.05$, $r_o/R^* = 0.01$, $r_o/R^* = 0.001$, and $r_o/R^* = 0.0001$. For the highest $r_o/R^*$, the transition is from the stretched lamellar (lamellar morphology with unfavorable geometric constraints resulting in high free energy) to bicontinuous morphology. For lower values of $r_o/R^*$, the transitions are between low free energy lamellar and bicontinuous phases and are therefore independent of the value of $r_o/R^*$. The free energy of the bicontinuous morphology does not change with $r_o$ because there is no compression in the bicontinuous morphology occurring for the given value of $k_\gamma$.

small values of $r_o/R^*$, the transitions are between the unstretched lamellar case, whereas $r_o/R^* = 0.05$ gives a transition between a normal lamellar and the bicontinuous morphology. The B → C and C → S transitions do not depend on $r_o/R^*$, but the reverse transitions (at higher values of $k_\phi$) do. Therefore, the lower left corner of the phase diagrams remains unchanged when the value of $r_o/R^*$ is changed because this region is dominated by a weak tendency of stretching for the curved morphologies, and thereby the polymers do not encounter compression.

The existence of both a cylindrical and a bicontinuous morphology beyond the existence of a spherical phase for very asymmetric, rigid copolymers is a tendency not observed when "loosening" the sharp interface constraint. So the thermodynamically stable morphologies (and thereby the curvatures) are clearly a result of the interplay between relative interfacial energies and the compositional polymer asymmetry.

From Figure 7, it can furthermore be seen that when the copolymer is softened overall (i.e., $r_o/R^*$ is decreased), the lamellar morphology becomes more and more dominant for log $k_\gamma \geq -1/2$. At the same time, the spherical morphology becomes more and more dominant for log $k_\gamma \leq -1$ because the tendency of compression of the outer component decreases when the copolymer becomes softer.

The Fredrickson asymmetry parameter takes into account different stiffnesses of the two copolymer parts. A value of $\epsilon_F < 1$ indicates that the end-to-end distance per volume of the core (B) component is larger than that of the outer component in the equilibrium condition with just one single copolymer. In Figure 9, the effect of $\epsilon_F$ on a copolymer with low extension (i.e., close to spherical "mushroom" conditions of both parts)

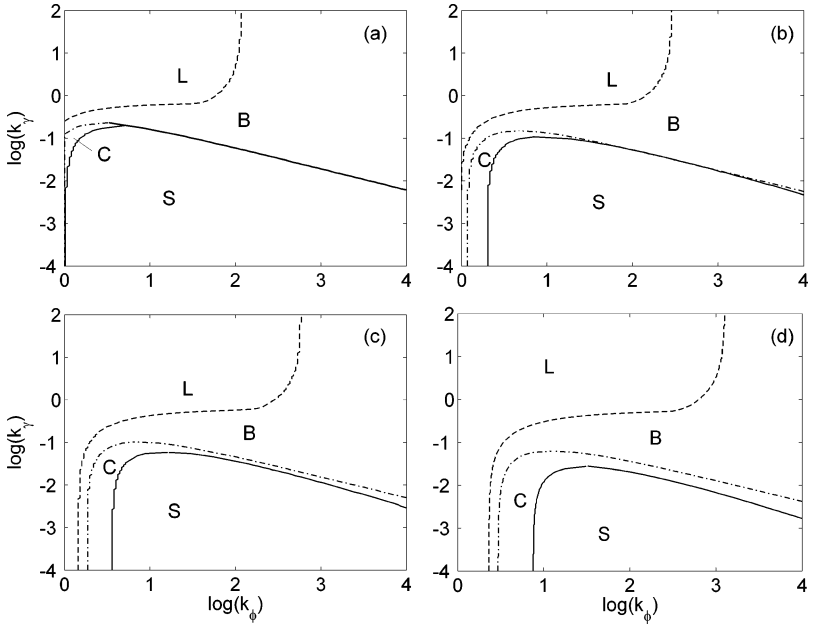


**Figure 9.** Phase diagrams for different values of the Fredrickson asymmetry parameter $\epsilon_F$ for a soft copolymer ($r_o/R^* = 0.0001$). (a) $\epsilon_F = 0.1$, (b) $\epsilon_F = 0.25$, (c) $\epsilon_F = 0.5$, (d) $\epsilon_F = 1$. The two upper systems with high stiffness asymmetry show directly transitions between the ordered bicontinuous and the spherical phases, whereas the transitions in the systems with lower stiffness gradually changes through the morphology sequence.

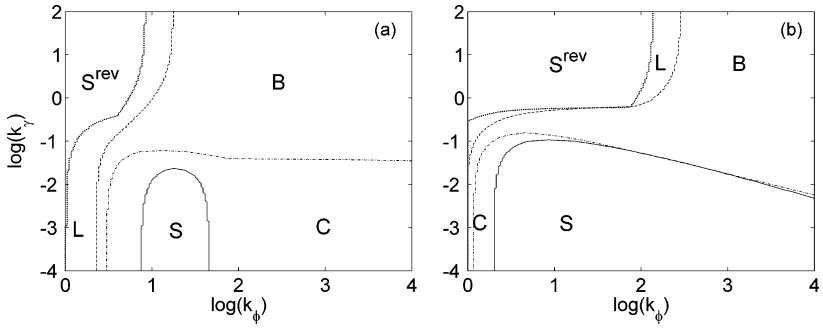


**Figure 10.** Morphology diagrams with the reversed spherical geometry taken into account for two different systems: (a) Coexistence between maximum two morphologies for a relatively rigid, stiffness symmetric copolymer ($R_o/R^* = 0.05$, $\epsilon_F = 1$) and (b) coexistence of several ($S^{rev}-L-B$ and $B-C-S$) morphologies for a soft, stiffness asymmetric copolymer ($R_o/R^* = 0.0001$, $\epsilon_F = 0.25$). $\gamma_o = \Omega = 1$, and $\phi_o = 0.01$

$r_o/R^* = 0.0001$ can be seen. A stiffer core component favors as expected the spherical morphology, and with a large degree of stiffness asymmetry ($\epsilon_F = 0.1$), it can be seen that for all values of $k_\phi > 10$ there is a direct transition between the spherical and the bicontinuous morphology. For $\epsilon_F = 0.25$, this transition is not direct but is in close equilibrium with the cylindrical morphology as well. For larger values of $\epsilon_F$, the transitions return to the traditional sequence where no phases are "omitted".

In Figure 10, two different scenarios are shown where the reversed spherical geometry morphology is included in the mapping. It is clear from previous results that the reversed spherical phase is in competition with the lamellar morphology when the A−S interfacial tension is high and is in general thermodynamically more favorable for $k_\gamma \geq -1/2$ until the polymer becomes too asymmetric (because the geometrical constraints of $S^{rev}$ favors excess of the core component). The introduction of this morphology furthermore results in the prediction of interesting transitions. In scenario (a), there are transitions between two morphologies only, but for the more stiffness asymmetric and less rigid copolymer in scenario (b), there are transitions between three morphologies both at (i) relatively low volumetric asymmetry for high $k_\gamma$, where the phases $S^{rev}$, L, and B coexist for a range of volumetric asymmetries, and (ii) relatively high volumetric asymmetry and low $k_\gamma$, where S, C, and B coexist for a large range of volumetric asymmetries. Scenario (i) can be imagined as a bicontinuous sponge with a certain degree of excluded noncontinuous areas of spherical solvent inclusions. Scenario (ii) can be imagined as a system, which is continuous in solvent and where the structures of copolymer is very likely to be "branched sponge" or individual morphologies with "bone" structure comparable to the complex structure in the regime where the S, C, and B morphologies were in coexistence, which were discussed earlier.

The presented model maps the phases where B is restricted to the core component in both the micellar and reversed morphologies only because earlier we have specified that the surface tension of the B−S interface is much larger than that of the A−S interface (i.e., $\gamma_{BS} \gg \gamma_{AS}$). There will, however, be a large degree of symmetry around $k_\phi = 1$ if the respective surface tensions of the two copolymer species and the solvent are comparable, i.e., $\gamma_{AS} \simeq \gamma_{BS}$. If $\gamma_{AS} = \gamma_{BS}$ and $\epsilon_F = 1$, there will be complete inversion around $k_\phi = 1$, as seen for copolymer melts with $\epsilon_F = 1$.[9]

**3.2. Discussion of Model Limitations.** In the simple case of diblock copolymer melts, the calculations based on round unit cells provide lower bounds for the free energy because the model in itself does not take into account the imperfect packing of the unit cells. However, for dilute solutions where the copolymer is confined to the center of the reference geometry, this "packing error" vanishes. This is because we do not have

to deform the micelles or vesicles into a space-filling array as discussed in OM[9] because there is only solvent present in the outer part of the geometry. Of course, a refinement of the model would be to account for the slight increase in polymer concentration in the geometry when the amount of solvent disappearing from the geometry volume when filling out the "holes" resulting from the densest packing is accounted for. This would not change any of the results in any significant way. The calculations presented here are, however, still lower bounds because we impose energetically expensive sharp concentration gradients without taking the energy into account and we approximate the interfaces by flat surfaces such that curvature arises only from the assembly of the reference geometries.

The reversed morphology will, in addition, experience the "imperfect packing" problem, and it should be kept in mind that the free energies of the reversed structures are lower bounds in one more way than the other morphologies because the stretching free energy of the outer component does not include the additional stretching arising from the space-filling procedure discussed above.

## 4. Conclusion

In this study, we have developed a theory that describes assembly of diblock copolymer into micelles when dispersed in dilute and mutually poor solvent in the strong segregation limit. The solvent is assumed to be selective such that only component A and solvent interactions are allowed, in other words, the B−S interface tension is very much higher. We have compared the free energy of four different phases (lamellar, ordered bicontinuous double-diamond, cylindrical, and spherical) and mapped their ranges of thermodynamic stability. The morphologies represent three solvent-continuous (S, C, and L) and one bicontinuous (B) phases, where the coexistence of two or more can explain the variety of complex copolymer structures found in experiments. The four micellar morphologies are furthermore compared to a "Swiss cheese" morphology ($S^{rev}$), where the copolymer is continuous but the solvent is limited to spherical inclusions, and this morphology is found to dominate when the A−S interface is very unfavorable and the polymer is relatively symmetric.

We include a compressional term into the traditional melt model of Olmsted and Milner, such that mathematical solutions arising from the simple extension of the model to polymeric solutions do not lead to situations where either of the two brushes is compressed. Because compressional forces are in general larger than extensional forces, we force the morphology to the compression threshold of the compressed part and calculate the free energy of this configuration, which we denote by "stretched". Thereby we can predict transitions from, e.g., stretched lamellar to bicontinuous phases. The stretched lamellar to bicontinuous transition occurs in general for systems with high A−S interfacial energy; if the model extension is not applied, the lamellar morphology would dominate for all asymmetries in this regime due to the increase in stretching of the curved morphologies compared to the lamellar to obtain similar outer surface areas (3 times as much stretching for spherical compared to lamellar).

The free energy of micelles in the strong segregation limit includes four conventional components: the surface free energies of the A−S and A−B surfaces, respectively, and the stretching free energies of the A and B components. When the interfacial energy of the outer surface (A−S) is large, the only curved morphology occurring is the bicontinuous at highly asymmetric copolymers. When the A−B interfacial energy is lower than that of the A−S interface, curved morphologies become preferable, but in contrast to copolymer melts and copolymer solutions in the weak segregation limit, the preferred morphology for large asymmetries (and asymmetries going toward infinity) is not the spherical micelle because that tends to compress the core component. It is, however, favored at intermediate asymmetries, and for copolymers with a rigid core component and an outer component in excess, the spherical geometry dominates the picture at $k_\gamma < 1$ with small domains of the bicontinuous morphology.

Experimental studies have indicated that in general there is coexistence of tubular, spherical, vesicular, and more complicated species in dilute solutions.[6,16] This can very easily be explained from the model because the free energies of the various phases in certain regimes are very close and therefore the thermodynamic equilibrium is never really reached. Furthermore, we have shown how several morphologies coexist at certain conditions leading to complex structures, which can be continuous in either component or in both.

This study gives evidence that, for dilute solutions of hydrophobic diblock copolymers in the strong segregation limit, the thermodynamically stable phases are not only determined from the asymmetry of the copolymer but to a large extent also by the ratio of the two surface energies. It is shown that even very asymmetric copolymers can exist in the lamellar morphology when the A−S interfacial energy is high compared to that of the A−B interface.

**Acknowledgment.** This research has been made possible by grants from Carlsbergfondet and EPSRC TCM/C3 Portfolio.

## Appendix

From simple scaling arguments, it can be shown that the monolayer vesicle in either reference geometry is not a thermodynamically stable morphology in the strong segregation limit. The monolayer vesicle is defined by three dividing surfaces, and if we investigate the regime $k_\phi \geq 1$ and give a value to the surface tension between solvent and B component $\gamma_{BS} \geq \gamma_{AS}$ rather than stating that the component B and solvent are completely immiscible, we can simplify the cylindrical monolayer vesicle always to form with the B component in the inner part of the geometry because B is the minority component and the BS interface is less favorable than the AS interface. If we choose the minimizing parameter to be the relative position of the inner (BS) surface, $\beta_1$, we then have to minimize over the physical values, i.e., $\beta_1 \in [0, \sqrt{1-\phi}]$. For $\beta_1 = 0$, we have the simple micellar case, and for $\beta_1 = \sqrt{1-\phi}$, we have the reversed cylindrical micelle with the components A and B inverted, which however does not change the calculations because we fix $\gamma_{AS} = \gamma_{BS}$. The volume balances over the B component and the entire copolymer in a cylindrical reference geometry then give the relative positions of the two outer dividing surfaces as function of that of the inner:

$$\beta_2 = \sqrt{\beta_1^2 + \phi_B} \tag{48}$$

$$\beta_3 = \sqrt{\beta_1^2 + \phi} \tag{49}$$

The free energy scales as $F \sim (K_{int})^{2/3}(K_{str})^{1/3}$, which then can be expressed as function of $\beta_1$:

$$F \sim \left(\beta_1\gamma_{BS} + \sqrt{\beta_1^2 + \phi_B}\gamma_{AB} + \mu(\beta_1)\sqrt{\beta_1^2 + \phi}\gamma_{AS}\right)^{2/3} \times (I_A^* + I_B^*)^{1/3} \tag{50}$$

where the function $\mu$ ensures that we do not calculate an interfacial energy for the AS surface in the case where the A component is restricted to the outer part of the reference geometry:

$$\mu(\beta_1) = 1 \text{ if } \beta_1 < \sqrt{1-\phi} \tag{51}$$

$$\mu(\beta_1) = 0 \text{ if } \beta_1 = \sqrt{1-\phi} \tag{52}$$

and the stretching integrals are given by:

$$I_A^* = \frac{3}{4}\left[\sqrt{\beta_1^2+\phi} - \sqrt{\beta_1^2+\phi_B}\right]^4 + \sqrt{\beta_1^2+\phi_B}\left[\sqrt{\beta_1^2+\phi} - \sqrt{\beta_1^2+\phi_B}\right]^3 \tag{53}$$

$$I_B^* = -\frac{3}{4}\left[\sqrt{\beta_1^2+\phi_B} - \beta_1\right]^4 + \sqrt{\beta_1^2+\phi_B}\left[\sqrt{\beta_1^2+\phi_B} - \beta_1\right]^3 \tag{54}$$

The free energy in different scenarios can be shown to have local maxima in the interval $\beta_1 = [0,(1-\phi)^{1/2}]$, but no local minima except for $\beta_1 = 0$ or $\beta_1 = (1-\phi)^{1/2}$. When $\gamma_{BS} = \gamma_{AB} = \gamma_{AS}$, the regular micellar structure is thermodynamically more favorable, i.e., the lowest free energy of the monolayer vesicle is obtained for $\beta_1 = 0$. This is also the case when $\gamma_{AB} \geq \gamma_{AS}$ and $\gamma_{BS} = \gamma_{AS}$. For $\gamma_{AB} \leq \gamma_{AS}$ and $\gamma_{BS} = \gamma_{AS}$, we find that the reverse spherical morphology (i.e., obtained for $\beta_1 = (1-\phi)^{1/2}$) is the most favorable, as we also showed in Figure 5 for the spherical morphology.

The same scaling arguments, with the appropriate area functions and volume balances replaced, can be used to show that neither the spherical nor the bicontinuous geometry favors a monolayer vesicular morphology compared to a micellar morphology.

## References and Notes


(1) Bates, F. S.; Fredrickson, G. H. *Annu. Rev. Phys. Chem.* **1990**, *41*, 525.
(2) Bates, F. S. *Science* **1991**, *251*, 898.
(3) Alberts, B.; Johnson, A.; Lewis, J.; Raff, M.; Roberts, K.; Walter, P. *Molecular Biology of the Cell*, 4th ed.; Garland Science, New York, 2002.
(4) Olmsted, P. D. In *Soft Condensed Matter Physics in Molecular and Cell Biology*, 1st ed.; Taylor and Francis Group, Boca Raton, FL, 2006.
(5) Discher, B. M.; Won, Y.-Y.; Ege, D. S.; Lee, J. C.-M.; Bates, F. S.; Discher, D. E.; Hammer, D. A. *Science* **1999**, *284*, 1143.
(6) Jain, S.; Bates, F. S. *Science* **2003**, *300*, 460.
(7) Safran, S. In *Statistical Thermodynamics of Surfaces, Interfaces and Membranes*, 1st ed.; Addison-Wesley: Reading, MA, 1994.
(8) Zhulina, E. B.; Adam, M.; LaRue, I.; Sheiko, S. S.; Rubinstein, M. *Macromolecules* **2005**, *38*, 5330.
(9) Olmsted, P. D.; Milner, S. T. *Macromolecules* **1998**, *31*, 4011.
(10) Bates, F. S.; Fredrickson, G. H. *Macromolecules* **1994**, *27*, 1065.
(11) Olmsted, P. D.; Milner, S. T. *Phys. Rev. Lett.* **1994**, *72*, 936.
(12) Helfand, E.; Tagami, Y. *J. Polym. Sci., Part B: Polym. Phys.* **1971**, *9*, 741.
(13) Semenov, A. N. *JETP Lett.* **1985**, *88*, 1242.
(14) Milner, S. T.; Witten, T. A.; Cates, M. E. *Macromolecules* **1988**, *21*, 2610.
(15) Milner, S. T.; Witten, T. A.; Cates, M. E. *Europhys. Lett.* **1988**, *5*, 413.
(16) Bang, J.; Jain, S.; Li, Z.; Lodge, T. P.; Pedersen, J. S.; Kesselman, E.; Talmon, Y. *Macromolecules* **2006**, *39*, 1199.
(17) Larsen, A. L.; Terentjev, E. M. *Macromolecules* **2006**, *39*, 9508.


MA061416L